

Article

High-Pressure Thermophysical Properties of Eight Paraffinic, Naphthenic, Polyalphaolefin and Ester Base Oils

Antía Villamayor^{1,2}, María J. G. Guimarey^{1,3}, Fátima Mariño¹, José M. Liñeira del Río^{1,4}, Francisco Urquiola⁵, Raquel Urchegui⁵, María J. P. Comuñas^{1,*} and Josefa Fernández¹ 

¹ Laboratory of Thermophysical and Tribological Properties, NaFoMat Group, Department of Applied Physics, Faculty of Physics and Institute of Materials (iMATUS), University of Santiago de Compostela, 15782 Santiago de Compostela, Spain

² Plasma Coating Technologies Unit, Tekniker, Basque Research and Technology Alliance (BRTA), c/Iñaki Goenaga 5, 20600 Eibar, Spain

³ Department of Design and Engineering, Faculty of Science & Technology, Bournemouth University, Talbot Campus, Poole BH12 5BB, UK

⁴ INEGI, Universidade do Porto, Faculdade de Engenharia, Rua Dr. Roberto Frias s/n, 4200-465 Porto, Portugal

⁵ Verkol S.A.U. Quaker Houghton, Polígono Zalain, 23 I, 31780 Bera Navarra, Spain

* Correspondence: mariajp.comunas@usc.es

Abstract: In this work, the thermophysical properties of four mineral (paraffinic and naphthenic) and four synthetic (polyalphaolefin and ester) base oils are measured. Knowledge of these properties is of vital importance for the correct and optimal formulation and design of lubricants, and for the development of equations of state and transport models that adequately represent their properties. Density, isothermal compressibility, thermal expansion coefficient, dynamic viscosity, pressure–viscosity coefficient, and contact angle were determined. To carry out this work, a pρT apparatus, a rotational viscometer, a falling body viscometer, and a contact angle analyzer were used. Highest densities were found for the polyalphaolefin and ester synthetic oils, increasing around 5% from 0.1 to 100 MPa for all the base oils. The density of the synthetic oils is less dependent on temperature changes. For the expansivity and compressibility of all the base oils, decreases with pressure of up to 35% and 45% were observed. From the contact angle measurements, it was observed that base oils with a higher viscosity grade have a worse wetting. The greatest effect of pressure on the dynamic viscosity was obtained for the naphthenic mineral oil and the lowest effect for the polyalphaolefin oil. Paraffinic and naphthenic oils present the highest universal pressure–viscosity coefficients.

Keywords: high pressure; mineral oils; synthetic oils; density; isothermal compressibility; thermal expansion coefficient; contact angle; dynamic viscosity; pressure–viscosity coefficient



Citation: Villamayor, A.; Guimarey, M.J.G.; Mariño, F.; Liñeira del Río, J.M.; Urquiola, F.; Urchegui, R.; Comuñas, M.J.P.; Fernández, J. High-Pressure Thermophysical Properties of Eight Paraffinic, Naphthenic, Polyalphaolefin and Ester Base Oils. *Lubricants* **2023**, *11*, 55. <https://doi.org/10.3390/lubricants11020055>

Received: 10 January 2023

Revised: 24 January 2023

Accepted: 28 January 2023

Published: 31 January 2023



Copyright: © 2023 by the authors. Licensee MDPI, Basel, Switzerland. This article is an open access article distributed under the terms and conditions of the Creative Commons Attribution (CC BY) license (<https://creativecommons.org/licenses/by/4.0/>).

1. Introduction

In accordance with the demands of society, modern development trends in the industry have shifted towards the use of biodegradable and low-toxicity synthetic lubricants, compared with petroleum-derived lubricants, in addition to lower emissions of organic volatile compounds [1,2]. Lubricants have a great impact on the energy efficiency, reliability, average life, and noise levels of industrial machinery [3]. In lubricant formulation, the selection of the base oils is of utmost importance [4]. Mineral-based oils are usually divided into paraffinic (PARA) and naphthenic (NAPH) depending on the chemical structure of the predominant component [5]. Synthetic base oils, such as polyalphaolefins (PAOs) and esters (ESTERS), are obtained by chemical synthesis, which makes it possible to achieve lubricants with very specific characteristics. Synthetic oils have another advantage over the former, i.e., they improve machine protection and maintain the stability of their properties for a longer period. Moreover, the low toxicity and excellent biodegradability of the ester base oils make them highly interesting from an environmental point of view [6].

For industrial applications, the knowledge of the lubricating properties and the thermophysical and tribological characterization of base oils of different nature (mineral, synthetic and vegetable oils) is essential. Knowledge of the density at high pressures is essential to determine the dynamic viscosity as a function of pressure and, subsequently, the pressure–viscosity coefficient and film thickness, parameters that are directly related to the proper selection of a lubricant for each application. Contact angle measurements (θ) are used to evaluate the tendency of the lubricants to spread on a solid surface (wetting ability), which is a key factor for many industrial processes involving two different phases and a very important factor affecting their lubrication performance [7]. The affinity of the lubricant to the surrounding surfaces is a system variable and, therefore, depends not only on the lubricant, but also on the contact surfaces. Properties such as foaming depend on the viscosity and surface tension of the lubricant [8]. Thus, it is crucial to have databases of the thermodynamic and transport properties, as well as equations of state and models that adequately represent these properties. Liquid lubricants are generally considered incompressible, even though their compressibility is an important property that varies with changes in temperature and pressure and must be taken into account in various cases, such as heavily loaded lubricated contacts or hydraulic fluid applications [9]. In hydraulic systems operating at high pressure, oils with low compressibility are required to transmit power efficiently, as low compressibility results in a fast response time, high-pressure transmission speed, and low power loss. However, a certain amount of compressibility is desirable because it dampens the pressure peaks caused by switching and thus provides a smoother operation [10]. For this reason, knowing the volumetric behavior of base oils at high pressures allows the evaluation of their degree of compressibility and thus helps in the development of more efficient lubricants for a particular application.

We have found in the literature several works studying the thermophysical and tribological properties of mineral and synthetic oils. Gold et al. [11] studied the viscosity–pressure–temperature behavior of several gear oils and hydraulic oils up to 0.8 GPa. Fernández Rico et al. [12] reported the contact angle of mineral and synthetic oils, showing that mineral oil has a higher value than that of synthetic oil. Grandelli et al. [13] determined the high-pressure volumetric properties of three commonly used poly(α -olefin) base oils, PAO 2, PAO 4, and PAO 8, using a special variable volume view cell, which permits continuous pressure scan and volume measurements. These authors [13] determined the densities at several temperatures and pressures up to 40 MPa. Dickmann et al. [14] carried out a comprehensive evaluation of the volumetric and viscous properties of various mineral and synthetic base oils. These authors used a variable volume display cell to obtain densities and a high-pressure rotational viscometer to obtain viscosities at shear rates between 480 and 1270 s⁻¹. Wang et al. [15] determined the pressure–viscosity coefficients of several mineral and synthetic oils with the aim of improving the rolling fatigue lives. Recently, Teh et al. [16] published a review on the tribological performance of non-water miscible lubricants, such as vegetable oil, blend oil, synthetic oil, and ionic liquids.

In order to analyze the effects of the chemical nature and of the viscosity grade on the thermophysical properties, the present work provides high-accurate experimental data on density, isothermal compressibility, thermal expansion coefficient, and viscosity over a temperature range from 278.15 to 373.15 K at a high pressure (up to 100 MPa for density and 150 MPa for viscosity) as well as contact angle values at atmospheric pressure of eight base lubricants. The thermophysical properties of the synthetic oils (polyalphaolefin and ester) are compared with those obtained for the mineral oils (paraffinic and naphthenic).

2. Experimental Procedure and Methodology

The base oils analyzed in this work were four mineral base oils and four synthetic base oils: two paraffinic oils (PARA#1 and PARA#2), two naphthenic oils (NAPH#1 and NAPH#2), two ester oils (ESTER#1 and ESTER#2), and two polyalphaolefin oils (PAO4 and PAO16). These lubricants were kindly provided by Verkol Lubricantes. PARA#1 and PARA#2 are paraffinic mineral solvent neutral classified as API Group I. NAPH#1 is a mid-

viscosity hydrotreated naphthenic base oil and NAPH#2 is a high viscosity hydrotreated naphthenic base. ESTER#1 is an adipic acid diester of long chain length alcohols and ESTER#2 is a mixture of adipic acid diester and pentaerythritol ester. NAPH#1, NAPH#2, ESTER#1 and ESTER#2 are categorized as API Group V. PAO4 is a low viscosity isoparaffinic polyalphaolefin and PAO16 is a mixture of high and low viscosity isoparaffinic polyalphaolefins. Both PAOs are classed as API Group IV. The eight base oils can be classified in two groups depending on their viscosity grade. Thus, the oils with kinematic viscosity around $20 \text{ mm}^2 \text{ s}^{-1}$, at 313.15 K and 0.1 MPa (low-viscosity grade, ISO VG22) were PARA#1, NAPH#1, ESTER#1, and PAO4, and those with kinematic viscosity, at 313.15 K and 0.1 MPa, around $100 \text{ mm}^2 \text{ s}^{-1}$ (high-viscosity grade, ISO VG100) were PARA#2, NAPH#2, ESTER#2, and PAO16.

Densities (ρ) and viscosities (ν and η) at atmospheric pressure were measured with the expanded uncertainties of $5 \cdot 10^{-4} \text{ g cm}^{-3}$ and 1%, respectively, by using an Anton Paar Stabinger SVM3000 rotational viscometer (Anton Paar, Graz, Austria). A vibrating tube densimeter (HPM Anton Paar (Anton Paar, Graz, Austria)) was used to measure densities at high pressures with expanded uncertainties lower than $5 \cdot 10^{-3} \text{ g cm}^{-3}$. Dynamic viscosities (η) as a function of pressure were obtained with an uncertainty of 3.5% with a falling body viscometer. Contact angles (θ) were measured using the sessile drop method through a Phoenix MT(A) contact angle analyzer with an expanded uncertainty of 1° . Other details regarding the experimental setups of density [17], viscosity [18], and contact angle [19] have been further reported in previous articles.

For industry applications, it is useful to have a correlation that permits the interpolation of the density of these oils at temperatures and pressures different than those studied in this paper. For this reason, the density of each oil, as a function of both the temperature and the pressure, were correlated through the Tammann–Tait empirical equation of state:

$$\rho(T, p) = \frac{A_0 + A_1 T + A_2 T^2 + A_3 T^3}{1 - C \ln\left(\frac{B_0 + B_1 T + B_2 T^2 + p}{B_0 + B_1 T + B_2 T^2 + 0.1 \text{ MPa}}\right)} \quad (1)$$

Using basic thermodynamic relations, it is possible to obtain the thermal expansion coefficient (α_p) and isothermal compressibility (κ_T) from density data at different temperatures and pressures. Generally, these properties are used to provide more specific information on the dependence of fluid density on temperature and pressure. The thermal expansion coefficient describes the effect of the temperature on the density at a constant pressure, and is defined as follows:

$$\alpha_p = \frac{1}{V} \left(\frac{\partial V}{\partial T} \right)_p = -\frac{1}{\rho} \left(\frac{\partial \rho}{\partial T} \right)_p \quad (2)$$

where α_p is the volumetric thermal expansion coefficient, ρ the density, V the volume, T the temperature, and p the pressure. If Equation (1) is used to represent the surface $\rho(T, p)$ for each base oil, the isobaric thermal expansivity can be obtained as follows:

$$\alpha_p(p, T) = -\frac{A_1 + 2A_2 T}{\rho_0(T, 0.1 \text{ MPa})} - \frac{C(0.1 \text{ MPa} - p)}{(B(T) + p)(B(T) + 0.1 \text{ MPa})} \frac{B_1 + 2B_2 T}{\left[1 - C \ln\left(\frac{B(T) + p}{B(T) + 0.1 \text{ MPa}}\right)\right]} \quad (3)$$

Changes in volume that occur with changes in pressure are often characterized using the isothermal compressibility (κ_T), which is defined as:

$$\kappa_T = -\frac{1}{V} \left(\frac{\partial V}{\partial P} \right)_T = \frac{1}{\rho} \left(\frac{\partial \rho}{\partial P} \right)_T \quad (4)$$

If Equation (1) is used to represent the surface $\rho(T, p)$ for each base oil, the isothermal compressibility can be obtained as follows:

$$\kappa_T(p, T) = \frac{C}{(B_0 + B_1T + B_2T^2 + p) \left[1 - C \ln \left(\frac{B_0 + B_1T + B_2T^2 + p}{B_0 + B_1T + B_2T^2 + 0.1 \text{ MPa}} \right) \right]} \quad (5)$$

The estimated uncertainty for the thermal expansion coefficient and the isothermal compressibility are around $0.3 \cdot 10^{-4} \text{ K}^{-1}$ and $0.06 \cdot 10^{-4} \text{ MPa}^{-1}$, respectively. For each base oils, the experimental dynamic viscosity data as a function of pressure, $\eta(p)$, were fitted at each temperature to the following equation:

$$\eta(p) = \eta_0 \exp \left[A \ln \left(\frac{B + p}{B + 0.1 \text{ MPa}} \right) \right] \quad (6)$$

where η_0 is the dynamic viscosity value obtained with the Anton Paar Stabinger viscometer at 0.1 MPa at each temperature) and A, B, and C are adjustable parameters. From Equation (6), it is possible to calculate the pressure–viscosity coefficient (α), which is another relevant property in lubrication [20–23]. In the present work, the procedure proposed by Bair et al. [23] was used to determine the pressure–viscosity coefficient using these equations:

$$\alpha = \alpha_{film} = \frac{1 - \exp(-3)}{p_{iv}(3/\alpha^*)} \quad (7)$$

where p_{iv} the isoviscous pressure given by:

$$p_{iv} = \int_0^{p''} \frac{\eta(p' = 0) dp'}{\eta(p')} \quad (8)$$

and α^* is the reciprocal asymptotic isoviscous pressure coefficient:

$$\alpha^* = \frac{1}{p_{iv}(\infty)} = \left[\int_0^\infty \frac{\eta(p = 0) dp}{\eta(p)} \right]^{-1} \quad (9)$$

The pressure–viscosity coefficient for the eight base oils was also estimated from the following equation proposed by Gold et al. [11], which relates this coefficient with the kinematic viscosity, v , at 0.1 MPa:

$$\alpha_{Gold} = sv^t \quad (10)$$

Gold et al. [11] used a database of 28 lubricants, including mineral, synthetic, and vegetable oils, to determine s and t values for six lubricant types. These parameters are valid from 278.15 to 353.15 K. There are several studies [23,24] concerning the relation between the pressure–viscosity coefficient (α) and the central film thickness (h_0). According to the American Gear Manufacturers Association (AGMA), under full-film elastohydrodynamic lubrication at speed U , the central film thickness is given by:

$$h_0 = f \eta_0^{0.69} \alpha^{0.56} U^{0.69} \quad (11)$$

where the parameter f is a function of the surface geometry, the applied load, and the elastic parameters of the rolling elements, and η_0 is the dynamic viscosity at atmospheric pressure. In Equation (11), for α , we chose the universal pressure–viscosity coefficient (α_{film}) obtained from Equation (7), as in a previous work [25]. From Equation (11), it can be concluded that, at a fixed temperature, comparing fluids with the same viscosity, the base oils that provide a better protection (thicker film) at extreme pressures are those with a higher pressure–viscosity coefficient. Nevertheless, to ensure a better efficiency, other factors should be considered, such as the reduction in wear, friction, sub-surface stress and pressure peaks [26–28]. Moreover, that the film thickness changes as little as possible with the temperature is desirable.

3. Results and Discussion

Table 1 reports the densities at 0.1 MPa from 278.15 to 373.15 K for the eight oils measured with the SVM3000 apparatus (Anton Paar, Graz, Austria). As can be seen in Figure 1, the densities of all eight base oils decrease linearly with increasing temperature at atmospheric pressure. The following sequence is observed for the density at atmospheric pressure for both groups, the low-viscosity-grade base oils (NAPH#1, PARA#1, PAO4, and ESTER#1) and the high-viscosity-grade base oils (NAPH#2, PARA#2, PAO16, and ESTER#2): ESTER > NAPH > PARA > PAO. Thus, at atmospheric pressure, the polyalphaolefin oils (PAO4 and PAO16) have the lowest density values, followed by the mineral base oil PARA#1. On the contrary, esters are the densest fluids in each group. At 0.1 MPa, the decrease in density from 278.15 to 373.15 K is around 7% for all the base oils.

Table 1. Density, ρ , kinematic viscosity, ν , and dynamic viscosity, η , for the eight base oils at different temperatures, T/K , and at 0.1 MPa measured with SVM3000 Stabinger.

T/K	$\rho/g\text{ cm}^{-3}$	$\nu/\text{mm}^2\text{ s}^{-1}$	$\eta/\text{mPa s}$	T/K	$\rho/g\text{ cm}^{-3}$	$\nu/\text{mm}^2\text{ s}^{-1}$	$\eta/\text{mPa s}$
<i>PARA#1</i>				<i>PARA#2</i>			
278.15	0.8695	99.41	86.44	278.15	0.8984	1403.3	1260.6
283.15	0.8664	73.32	63.53	283.15	0.8953	913.2	817.6
288.15	0.8633	55.44	47.86	288.15	0.8923	614.3	548.1
293.15	0.8601	42.80	36.82	293.15	0.8892	424.9	377.8
298.15	0.8570	33.66	28.85	298.15	0.8862	301.2	266.9
303.15	0.8538	26.94	23.00	303.15	0.8832	218.5	192.9
308.15	0.8506	21.90	18.63	308.15	0.8802	161.8	142.4
313.15	0.8475	18.07	15.31	313.15	0.8772	122.3	107.2
318.15	0.8443	15.10	12.75	318.15	0.8742	94.06	82.23
323.15	0.8411	12.77	10.74	323.15	0.8712	73.60	64.12
328.15	0.8379	10.92	9.152	328.15	0.8682	58.50	50.79
333.15	0.8347	9.428	7.870	333.15	0.8651	47.17	40.81
338.15	0.8315	8.217	6.832	338.15	0.8620	38.55	33.23
343.15	0.8283	7.217	5.978	343.15	0.8590	31.91	27.41
348.15	0.8251	6.388	5.271	348.15	0.8559	26.73	22.87
353.15	0.8218	5.693	4.679	353.15	0.8528	22.60	19.27
358.15	0.8186	5.107	4.181	358.15	0.8497	19.31	16.40
363.15	0.8154	4.607	3.757	363.15	0.8467	16.64	14.09
368.15	0.8122	4.179	3.394	368.15	0.8436	14.46	12.20
373.15	0.8089	3.807	3.080	373.15	0.8405	12.66	10.64
<i>NAPH#1</i>				<i>NAPH#2</i>			
278.15	0.9072	206.2	187.1	278.15	0.9227	2174.4	2006.3
283.15	0.9040	136.3	123.2	283.15	0.9196	1261.5	1160.1
288.15	0.9009	93.87	84.57	288.15	0.9165	768.3	704.1
293.15	0.8977	66.85	60.02	293.15	0.9133	487.3	445.1
298.15	0.8945	49.05	43.88	298.15	0.9103	320.5	291.7
303.15	0.8914	36.98	32.96	303.15	0.9072	218.0	197.7
308.15	0.8882	28.56	25.37	308.15	0.9041	152.8	138.1
313.15	0.8849	22.54	19.94	313.15	0.9011	110.1	99.20
318.15	0.8817	18.12	15.98	318.15	0.8980	81.37	73.07
323.15	0.8785	14.83	13.02	323.15	0.8949	61.54	55.07
328.15	0.8752	12.31	10.78	328.15	0.8918	47.53	42.39
333.15	0.8720	10.37	9.046	333.15	0.8887	37.43	33.26
338.15	0.8687	8.840	7.679	338.15	0.8855	29.97	26.54
343.15	0.8655	7.614	6.590	343.15	0.8824	24.39	21.52
348.15	0.8622	6.626	5.713	348.15	0.8793	20.13	17.70

Table 1. Cont.

<i>T/K</i>	$\rho/\text{g cm}^{-3}$	$\nu/\text{mm}^2 \text{ s}^{-1}$	$\eta/\text{mPa s}$	<i>T/K</i>	$\rho/\text{g cm}^{-3}$	$\nu/\text{mm}^2 \text{ s}^{-1}$	$\eta/\text{mPa s}$
353.15	0.8589	5.815	4.995	353.15	0.8761	16.83	14.75
358.15	0.8557	5.142	4.400	358.15	0.8730	14.24	12.43
363.15	0.8524	4.586	3.909	363.15	0.8698	12.17	10.59
368.15	0.8491	4.114	3.493	368.15	0.8667	10.51	9.109
373.15	0.8458	3.712	3.140	373.15	0.8635	9.156	7.907
	<i>ESTER#1</i>				<i>ESTER#2</i>		
278.15	0.9202	158.8	146.1	278.15	0.9299	844.6	785.4
283.15	0.9168	114.6	105.0	283.15	0.9266	584.1	541.3
288.15	0.9134	85.03	77.67	288.15	0.9233	415.2	383.3
293.15	0.9100	64.64	58.82	293.15	0.9200	301.9	277.7
298.15	0.9066	50.22	45.53	298.15	0.9168	224.2	205.6
303.15	0.9032	39.74	35.89	303.15	0.9135	170.0	155.3
308.15	0.8998	32.02	28.81	308.15	0.9103	131.2	119.4
313.15	0.8964	26.20	23.49	313.15	0.9071	103.0	93.39
318.15	0.8930	21.75	19.43	318.15	0.9039	82.08	74.18
323.15	0.8896	18.29	16.28	323.15	0.9006	66.37	59.77
328.15	0.8862	15.56	13.79	328.15	0.8974	54.37	48.79
333.15	0.8828	13.38	11.81	333.15	0.8941	45.10	40.32
338.15	0.8793	11.61	10.21	338.15	0.8909	37.82	33.69
343.15	0.8759	10.17	8.905	343.15	0.8876	32.04	28.44
348.15	0.8725	8.969	7.825	348.15	0.8843	27.41	24.24
353.15	0.8690	7.969	6.926	353.15	0.8811	23.65	20.84
358.15	0.8656	7.129	6.171	358.15	0.8778	20.59	18.07
363.15	0.8621	6.415	5.530	363.15	0.8745	18.03	15.77
368.15	0.8587	5.804	4.984	368.15	0.8712	15.91	13.86
373.15	0.8552	5.277	4.513	373.15	0.8680	14.13	12.26
	<i>PAO4</i>				<i>PAO16</i>		
278.15	0.8252	82.54	68.11	278.15	0.8439	826.8	697.8
283.15	0.8221	63.20	51.96	283.15	0.8409	590.1	496.2
288.15	0.8190	49.31	40.38	288.15	0.8379	430.7	360.9
293.15	0.8159	39.10	31.90	293.15	0.8349	320.6	267.7
298.15	0.8128	31.47	25.58	298.15	0.8319	243.0	202.2
303.15	0.8097	25.68	20.79	303.15	0.8289	187.3	155.3
308.15	0.8065	21.23	17.12	308.15	0.8259	146.6	121.1
313.15	0.8034	17.76	14.27	313.15	0.8230	116.4	95.83
318.15	0.8003	15.02	12.02	318.15	0.8200	93.71	76.84
323.15	0.7971	12.83	10.23	323.15	0.8170	76.36	62.39
328.15	0.7939	11.06	8.782	328.15	0.8140	62.95	51.24
333.15	0.7908	9.616	7.604	333.15	0.8109	52.41	42.50
338.15	0.7876	8.504	6.698	338.15	0.8079	44.11	35.63
343.15	0.7844	7.466	5.857	343.15	0.8049	37.46	30.15
348.15	0.7812	6.627	5.177	348.15	0.8018	32.09	25.73
353.15	0.7780	5.919	4.605	353.15	0.7988	27.72	22.14
358.15	0.7749	5.319	4.121	358.15	0.7957	24.13	19.20
363.15	0.7717	4.802	3.706	363.15	0.7927	21.15	16.76
368.15	0.7685	4.359	3.350	368.15	0.7897	18.64	14.72
373.15	0.7653	3.976	3.043	373.15	0.7866	16.53	13.00

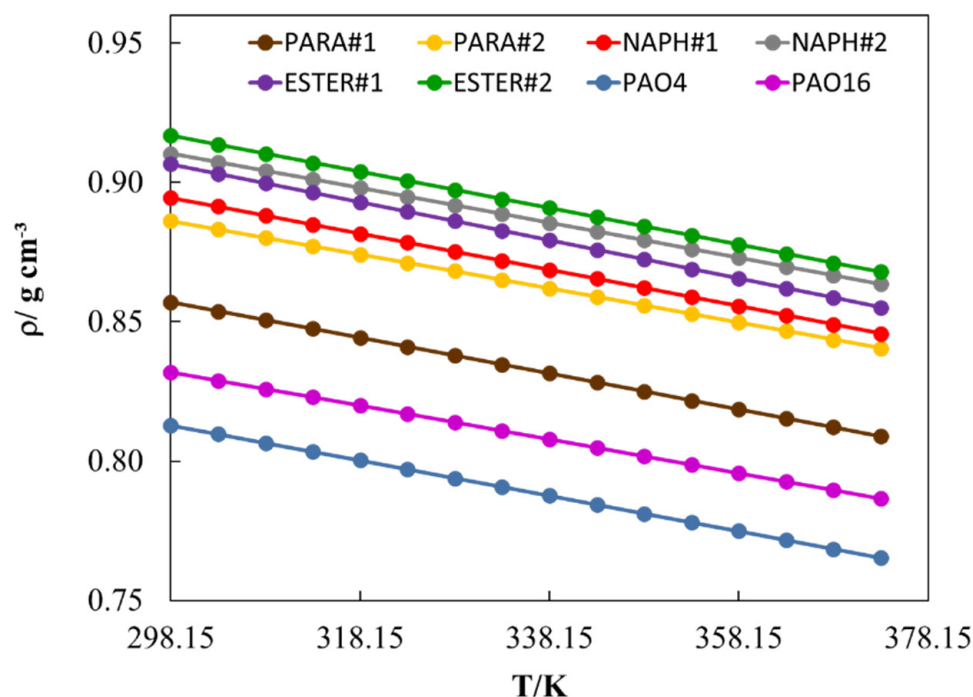


Figure 1. Densities, ρ , obtained with the SVM300 apparatus at 0.1 MPa for the eight oils versus the temperature function. The solid lines are for guidance.

The experimental results of the densities at high pressures for the mineral and synthetic base oils are reported in Table 2 at a temperature range from 298.15 to 373.15 K and at pressures up to 100 MPa. The density values measured with the $p\rho T$ apparatus at 0.1 MPa for the eight base oils were compared with those obtained with SVM3000 Stabinger apparatus over the temperature interval from 298.15 to 373.15 K. Relative deviations between 0.03% and 0.12% for the temperature of 298.15 K and from 0.01% to 0.08% for the highest temperature, 373.15 K, were found. These good results (very-low relative deviations between both apparatuses) are also a way to check and confirm the reliability of the $p\rho T$ apparatus. The density of the eight base oils varies from 0.7646 to 0.9600 g cm⁻³ during the entirety of the pressure and the temperature interval. In Figure 2a, the density of all the base oils was plotted at a fixed pressure (60 MPa) against the temperature. This figure can be compared with Figure 1, where the data obtained with the SVM3000 apparatus at a low pressure (0.1 MPa) are also plotted as a function of the temperature. The same trend with temperature was observed for all the base oils over both isobars (0.1 and 60 MPa). It was found that, at a fixed temperature, the ESTER#2 oil has the highest densities in the entire pressure range; so, for example, at 333.15 K, the density of this oil changes from 0.8934 g cm⁻³ at 0.1 MPa to 0.9422 g cm⁻³ at 100 MPa. On the contrary, PAO4 has the lowest densities, ranging from 0.7896 g cm⁻³ at 0.1 MPa to 0.8400 g cm⁻³ at 100 MPa at the same temperature. For all the temperatures and pressures, the densities of the polyalphaolefins are around 11% (PAO4) and 9% (PAO16) lower than those of ESTER#2. The other synthetic oil (ESTER#1) has densities slightly lower (around 1%) than those of ESTER#2. Concerning mineral oils, naphthenic oils have higher densities than paraffinic oils. In Figure 2b, the dependence of the density with pressure is plotted at 333.15 K for the eight oils. Densities at 100 MPa are around 5% higher than those at 0.1 MPa for all the base oils for all the isotherms. This increase in density due to pressure must be considered in the design of the machinery that works under high loads.

The coefficients A_i ($i = 0, 1, 2$) of Equation (1) were determined for each base oil in a preliminary fit of the density at 0.1 MPa as a function of the temperature. The coefficients B_j ($j = 0, 1, 2$) and C were fitted to the density measurements, at pressures different than 0.1 MPa, using the Levenberg–Marquardt algorithm. The parameter values are presented

in Table 3. Comparing the experimental density data and those obtained from Equation (1), we can observe that yield standard deviations (σ) are lower than $6.5 \cdot 10^{-4} \text{ g cm}^{-3}$, which is a measure of the dispersion of the data. The σ values for all the oils are lower than the estimated experimental uncertainty ($5 \cdot 10^{-3} \text{ g cm}^{-3}$). As an example, Figure 3 shows, for NAPH#2, the $\rho(T,p)$ surface obtained with Equation (1) together with the experimental data measured with the HPM densimeter.

Table 2. Experimental density data, $\rho/\text{g cm}^{-3}$, measured with the Anton Paar HPM densimeter of the eight base oils as a function of temperature (T) and pressure (P).

P/MPa	T/K							
	PARA#1	NAPH#1	ESTER#1	PAO4	PARA#2	NAPH#2	ESTER#2	PAO16
				298.15				
0.1	0.8573	0.8945	0.9065	0.8121	0.8870	0.9107	0.9168	0.8308
1	0.8578	0.8950	0.9070	0.8127	0.8875	0.9111	0.9173	0.8313
5	0.8601	0.8973	0.9093	0.8150	0.8896	0.9132	0.9195	0.8335
10	0.8628	0.9000	0.9121	0.8178	0.8922	0.9158	0.9221	0.8362
20	0.8681	0.9052	0.9175	0.8232	0.8971	0.9207	0.9272	0.8412
40	0.8777	0.9148	0.9276	0.8328	0.9061	0.9298	0.9367	0.8504
60	0.8863	0.9234	0.9368	0.8415	0.9143	0.9380	0.9453	0.8587
80	0.8942	0.9313	0.9449	0.8494	0.9218	0.9455	0.9531	0.8665
100	0.9016	0.9386	0.9521	0.8571	0.9287	0.9525	0.9600	0.8744
				313.15				
0.1	0.8473	0.8845	0.8958	0.8024	0.8774	0.9008	0.9069	0.8219
1	0.8479	0.8850	0.8964	0.8030	0.8779	0.9013	0.9074	0.8225
5	0.8503	0.8874	0.8988	0.8055	0.8801	0.9036	0.9097	0.8248
10	0.8532	0.8903	0.9017	0.8085	0.8829	0.9063	0.9125	0.8277
20	0.8588	0.8958	0.9074	0.8142	0.8881	0.9115	0.9179	0.8330
40	0.8689	0.9059	0.9181	0.8245	0.8976	0.9211	0.9279	0.8427
60	0.8780	0.9149	0.9278	0.8336	0.9062	0.9298	0.9370	0.8514
80	0.8863	0.9232	0.9365	0.8418	0.9141	0.9377	0.9452	0.8595
100	0.8939	0.9308	0.9443	0.8497	0.9213	0.9450	0.9525	0.8674
				333.15				
0.1	0.8340	0.8711	0.8819	0.7896	0.8646	0.8878	0.8934	0.8099
1	0.8347	0.8717	0.8824	0.7902	0.8651	0.8884	0.8939	0.8105
5	0.8373	0.8743	0.8850	0.7929	0.8676	0.8908	0.8964	0.8131
10	0.8405	0.8774	0.8881	0.7962	0.8705	0.8938	0.8994	0.8161
20	0.8465	0.8834	0.8942	0.8024	0.8762	0.8994	0.9052	0.8220
40	0.8574	0.8942	0.9056	0.8135	0.8864	0.9097	0.9161	0.8324
60	0.8671	0.9038	0.9161	0.8232	0.8956	0.9190	0.9259	0.8416
80	0.8758	0.9125	0.9255	0.8319	0.9039	0.9274	0.9346	0.8500
100	0.8838	0.9206	0.9340	0.8400	0.9115	0.9351	0.9422	0.8581
				348.15				
0.1	0.8242	0.8611	0.8716	0.7800	0.8551	0.8782	0.8834	0.8009
1	0.8248	0.8618	0.8722	0.7807	0.8557	0.8788	0.8840	0.8015
5	0.8276	0.8645	0.8749	0.7835	0.8583	0.8814	0.8866	0.8042
10	0.8310	0.8679	0.8781	0.7870	0.8614	0.8846	0.8898	0.8075
20	0.8375	0.8742	0.8845	0.7936	0.8674	0.8906	0.8960	0.8136
40	0.8489	0.8856	0.8965	0.8053	0.8782	0.9014	0.9074	0.8247
60	0.8591	0.8957	0.9075	0.8156	0.8877	0.9110	0.9177	0.8343
80	0.8682	0.9048	0.9175	0.8246	0.8964	0.9198	0.9268	0.8430
100	0.8764	0.9131	0.9265	0.8330	0.9043	0.9279	0.9347	0.8512
				353.15				
0.1	0.8209	0.8578	0.8682	0.7768	0.8519	0.8750	0.8801	0.7978
1	0.8215	0.8585	0.8688	0.7775	0.8525	0.8756	0.8807	0.7984
5	0.8244	0.8613	0.8715	0.7804	0.8552	0.8783	0.8834	0.8012
10	0.8279	0.8647	0.8748	0.7840	0.8584	0.8815	0.8866	0.8045
20	0.8345	0.8712	0.8813	0.7907	0.8645	0.8876	0.8929	0.8108

Table 2. Cont.

P/MPa	T/K							
	PARA#1	NAPH#1	ESTER#1	PAO4	PARA#2	NAPH#2	ESTER#2	PAO16
40	0.8462	0.8828	0.8934	0.8026	0.8754	0.8987	0.9046	0.8221
60	0.8564	0.8930	0.9046	0.8130	0.8852	0.9085	0.9150	0.8319
80	0.8657	0.9022	0.9148	0.8223	0.8940	0.9173	0.9242	0.8407
100	0.8740	0.9107	0.9241	0.8307	0.9020	0.9255	0.9323	0.8489
0.1	0.8083	0.8452	0.8553	0.7646	0.8400	0.8630	0.8677	0.7861
1	0.8084	0.8453	0.8554	0.7648	0.8400	0.8631	0.8678	0.7862
5	0.8116	0.8485	0.8582	0.7679	0.8429	0.8660	0.8706	0.7892
10	0.8154	0.8523	0.8617	0.7718	0.8464	0.8695	0.8742	0.7928
20	0.8225	0.8594	0.8686	0.7790	0.8530	0.8762	0.8809	0.7996
40	0.8351	0.8719	0.8815	0.7920	0.8647	0.8879	0.8933	0.8118
60	0.8461	0.8827	0.8934	0.8031	0.8750	0.8983	0.9044	0.8223
80	0.8558	0.8924	0.9044	0.8130	0.8843	0.9076	0.9141	0.8316
100	0.8646	0.9013	0.9144	0.8218	0.8927	0.9162	0.9225	0.8401

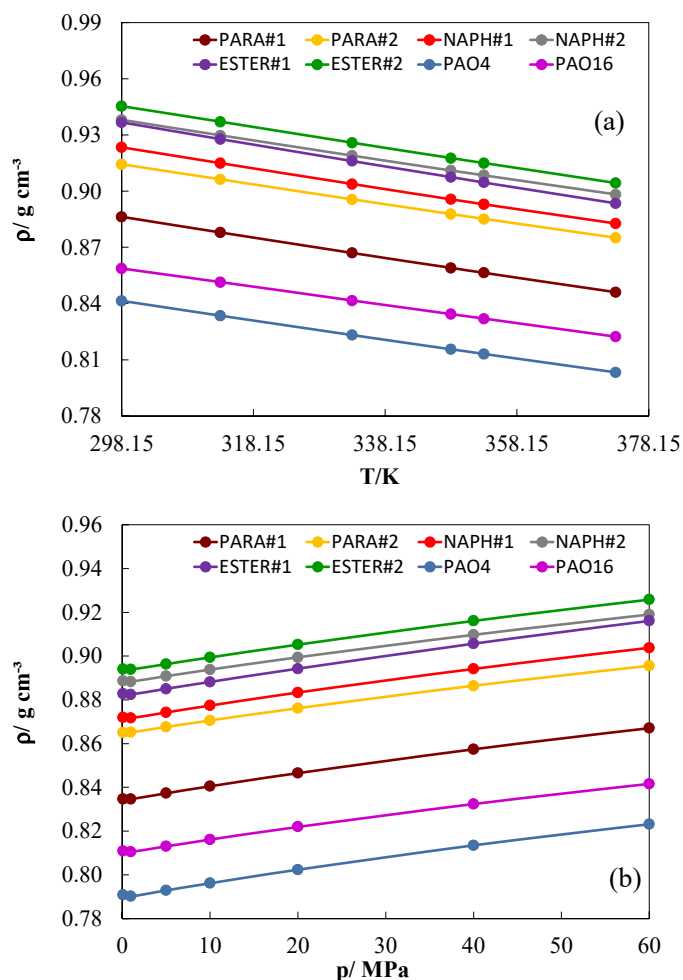


Figure 2. Density at high pressure obtained with the Anton Paar apparatus, (a) as a function of temperature at 60 MPa and (b) as a function of pressure at 333.15 K, for the eight base oils. The solid lines are for guidance.

Table 3. Parameters and deviations for density correlation by using Equation (1).

	PARA#1	NAPH#1	ESTER#1	PAO4	PARA#2	NAPH#2	ESTER#2	PAO16
$A_0/\text{g cm}^{-3}$	1.0340	1.0572	1.0704	1.0846	1.1016	1.1072	0.9887	1.0015
$10^4 \cdot A_1/\text{g cm}^{-3} \text{K}^{-1}$	-5.5605	-5.4302	-5.4231	-5.5306	-6.2946	-6.2849	-5.5574	-5.4016
$10^6 \cdot A_2/\text{g cm}^{-3} \text{K}^{-2}$	-0.1262	-0.1000	-0.1602	-0.1059	-0.0831	-0.0339	-0.1155	-0.0959
$10^2 \cdot C$	9.3732	8.9813	9.6793	9.6168	12.3161	9.6671	10.5167	10.6141
B_0/MPa	284.529	268.536	262.860	306.981	507.125	440.691	402.898	564.606
$B_1/\text{MPa K}^{-1}$	-0.4194	-0.3095	-0.1360	-0.3398	-1.1711	-1.1458	-0.9538	-1.7773
$10^3 \cdot B_2/\text{MPa K}^{-2}$	-0.1963	-0.3160	-0.7213	-0.4202	0.5354	0.7500	0.4325	0.1572
$10^4 \cdot \sigma/\text{g cm}^{-3}$	4.6	4.9	5.1	5.1	5.2	5.0	6.4	5.9
AAD/%	0.04	0.04	0.04	0.04	0.05	0.04	0.06	0.06
Bias/%	-0.02	-0.01	-0.03	-0.02	-0.02	-0.02	-0.04	-0.04
MD/%	0.14	0.13	0.13	0.12	0.10	0.11	0.16	0.13

AAD = average absolute deviation; Bias = average deviation; MD = maximum deviation.

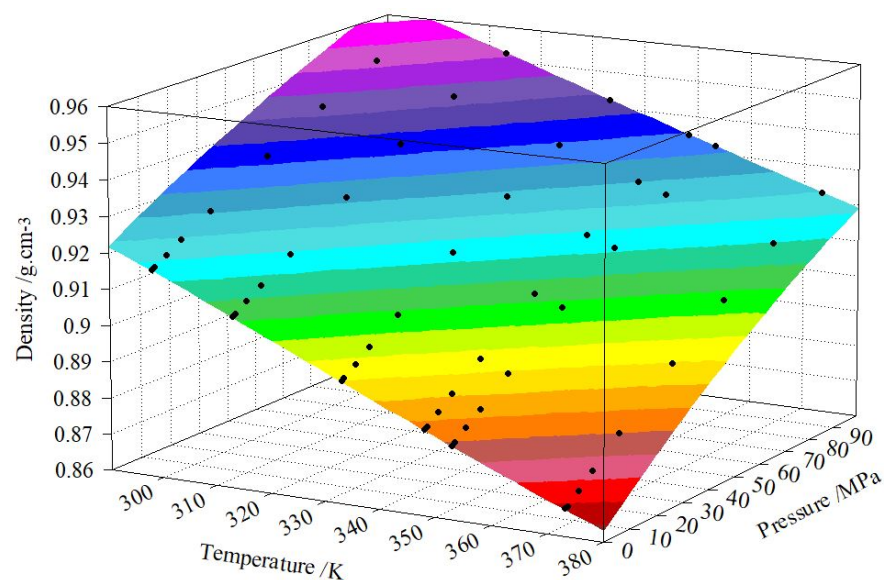


Figure 3. ρpT surface as a function of the temperature and pressure for NAPH#2 base oil. The dots represent the density measurements obtained with the Anton Paar apparatus, and the surface the correlation using Equation (1) with a standard deviation of $5 \cdot 10^{-4} \text{ g cm}^{-3}$.

The isobaric thermal expansivities and the isothermal compressibilities obtained for the eight base oils through Equations (3) and (5) and the values of coefficients A_i , B_i , and C from Table 3 are summarized in Tables 4 and 5, respectively. The decrease in the isobaric thermal expansivity from 0.1 MPa to 100 MPa for all the base oils is around 20% at 298.15 K and around 35% at 373.15 K. Thermal expansivities are depicted in Figures 4 and 5 as a function of the pressure at different temperatures for the mineral and synthetic base oils studied in this work. As remarked above, this property decreases when the pressure increases, whereas several crossing points are found between isotherms for all the base oils (around 40 MPa), except for PAO16. Although some authors [29–31] concluded that, for a given liquid, all the isotherms of α_p against pressure, cross at one definite pressure, Figures 4 and 5 show that this does not occur. This agrees with later articles [32,33], which found a clear dependence of the crossing pressure against temperature for some molecular liquids. For PAO16, the crossing points seem to be a little beyond the studied pressure range.

Table 4. Isobaric thermal expansivity, $\alpha_P / 10^{-4} \text{ K}^{-1}$, of eight base oils, as a function of temperature (T) and pressure (P).

P/MPa	T/K							
	PARA#1	NAPH#1	ESTER#1	PAO4	PARA#2	NAPH#2	ESTER#2	PAO16
				298.15				
0.1	7.4	6.8	7.1	6.8	7.5	7.1	7.7	7.2
5	7.3	6.7	7.0	6.7	7.4	7.0	7.5	7.0
20	6.9	6.4	6.7	6.4	7.0	6.6	7.2	6.7
60	6.3	5.9	6.2	5.9	6.3	6.0	6.4	5.8
100	5.8	5.5	5.7	5.5	5.7	5.5	5.8	5.2
				313.15				
0.1	7.5	6.9	7.3	6.9	7.6	7.2	7.8	7.3
5	7.4	6.8	7.1	6.8	7.5	7.0	7.7	7.1
20	7.0	6.5	6.8	6.5	7.1	6.7	7.2	6.7
60	6.3	5.9	6.1	5.9	6.3	6.0	6.4	5.9
100	5.8	5.5	5.7	5.4	5.7	5.4	5.7	5.2
				333.15				
0.1	7.7	7.1	7.4	7.0	7.8	7.3	8.0	7.5
5	7.5	6.9	7.3	6.9	7.6	7.1	7.8	7.3
20	7.1	6.6	6.9	6.5	7.2	6.7	7.3	6.8
60	6.3	5.9	6.1	5.8	6.3	5.9	6.3	5.9
100	5.7	5.4	5.5	5.3	5.6	5.4	5.6	5.2
				348.15				
0.1	7.8	7.2	7.6	7.1	7.9	7.4	8.1	7.6
5	7.6	7.0	7.4	7.0	7.7	7.2	7.9	7.4
20	7.1	6.6	6.9	6.6	7.2	6.8	7.4	6.9
60	6.2	5.8	6.0	5.7	6.2	5.9	6.2	5.9
100	5.6	5.3	5.4	5.2	5.5	5.3	5.5	5.2
				353.15				
0.1	7.9	7.2	7.6	7.2	7.9	7.4	8.2	7.6
5	7.7	7.0	7.4	7.0	7.7	7.2	8.0	7.4
20	7.1	6.6	6.9	6.6	7.2	6.8	7.4	6.9
60	6.2	5.8	6.0	5.7	6.2	5.9	6.2	5.9
100	5.5	5.3	5.3	5.1	5.4	5.3	5.4	5.2
				373.15				
0.1	8.0	7.4	7.8	7.3	8.1	7.5	8.4	7.8
5	7.8	7.2	7.6	7.1	7.9	7.3	8.1	7.6
20	7.2	6.7	6.9	6.6	7.3	6.8	7.4	7.0
60	6.0	5.7	5.7	5.6	6.1	5.8	6.1	5.9
100	5.2	5.1	4.9	4.9	5.2	5.2	5.2	5.2

The isothermal compressibility, κ_T , increases with the temperature at a constant pressure for all studied oils, whereas it decreases when the pressure rises at a constant temperature. The decrease in the isothermal compressibility from 0.1 MPa to 100 MPa for all the base oils is around 35% at 298.15 K and around 45% at 373.15 K. The more compressible base oil is ESTER#2, followed by PARA#1, for all the temperatures and pressures (Figure 6). The pressure and temperature dependence of the density and, subsequently, of the isothermal compressibility and thermal expansivity of the base oils must be considered to formulate new potential lubricants.

Table 5. Isothermal compressibility, $k_T/10^{-4} \text{ MPa}^{-1}$, of the eight base oils studied in this work.

P/MPa	T/K							
	PARA#1	NAPH#1	ESTER#1	PAO4	PARA#2	NAPH#2	ESTER#2	PAO16
				298.15				
0.1	6.59	6.06	6.12	5.71	5.99	5.83	6.70	6.08
5	6.40	5.88	5.95	5.56	5.87	5.68	6.51	5.93
20	5.86	5.40	5.50	5.16	5.52	5.26	6.02	5.52
60	4.80	4.45	4.58	4.34	4.79	4.41	5.02	4.67
100	4.08	3.79	3.94	3.75	4.24	3.81	4.32	4.06
				313.15				
0.1	6.99	6.38	6.47	6.03	6.38	6.22	7.17	6.54
5	6.77	6.19	6.28	5.87	6.24	6.04	6.96	6.37
20	6.17	5.66	5.78	5.42	5.86	5.58	6.40	5.90
60	5.01	4.62	4.78	4.52	5.04	4.63	5.28	4.94
100	4.23	3.92	4.08	3.89	4.43	3.98	4.51	4.27
				333.15				
0.1	7.61	6.89	7.04	6.53	6.98	6.79	7.89	7.22
5	7.35	6.66	6.82	6.34	6.81	6.59	7.64	7.01
20	6.65	6.05	6.23	5.83	6.36	6.04	6.97	6.44
60	5.32	4.88	5.08	4.80	5.41	4.95	5.67	5.32
100	4.45	4.11	4.30	4.10	4.72	4.21	4.79	4.55
				348.15				
0.1	8.16	7.33	7.55	6.98	7.49	7.28	8.53	7.78
5	7.86	7.07	7.30	6.76	7.30	7.05	8.23	7.54
20	7.06	6.39	6.63	6.18	6.78	6.42	7.46	6.89
60	5.58	5.10	5.35	5.04	5.71	5.20	5.99	5.62
100	4.64	4.27	4.50	4.27	4.95	4.39	5.02	4.77
				353.15				
0.1	8.37	7.49	7.75	7.14	7.68	7.45	8.76	7.98
5	8.05	7.22	7.48	6.92	7.48	7.21	8.45	7.72
20	7.22	6.51	6.78	6.31	6.93	6.55	7.64	7.04
60	5.68	5.18	5.44	5.12	5.82	5.29	6.10	5.73
100	4.70	4.32	4.56	4.33	5.03	4.46	5.11	4.84
				373.15				
0.1	9.30	8.23	8.66	7.90	8.51	8.22	9.80	8.82
5	8.91	7.91	8.33	7.62	8.26	7.92	9.42	8.51
20	7.90	7.07	7.47	6.89	7.60	7.14	8.42	7.69
60	6.10	5.53	5.88	5.51	6.29	5.67	6.60	6.15
100	4.99	4.56	4.87	4.60	5.38	4.72	5.45	5.15

The static contact angle evolution between the surface and a small drop of lubricant was analyzed by taking images at every second for 120 s (when the steady state was reached). Figure 7 shows the frames captured at 0, 60, and 120 s. The integrated software automatically calculates the angle that the lubricant drop forms with the steel surface on the right and left side and provides the average of both values. The analysis of the contact angle evolution of eight base oils on AISI 420 stainless steel surfaces showed that the base oils with a kinematic viscosity of around $100 \text{ mm}^2 \text{ s}^{-1}$, at 313.15 K and 0.1 MPa (PARA#2, NAPH#2, ESTER#2, and PAO16), have a higher contact angle than the base oils with a kinematic viscosity of around $20 \text{ mm}^2 \text{ s}^{-1}$, at 313.15 K and 0.1 MPa (PARA#1, NAPH#1, ESTER#1, and PAO4), which suggests the poorer wetting of the high-viscosity base oils. Furthermore, the wetting data for the high-viscosity base oils show the following sequence, PARA#2 > ESTER#2 > PAO16 > NAPH#2, which means that the highest contact angle is obtained for the paraffinic oil (PARA#2) and the lowest for the naphthenic oil (NAPH#2).

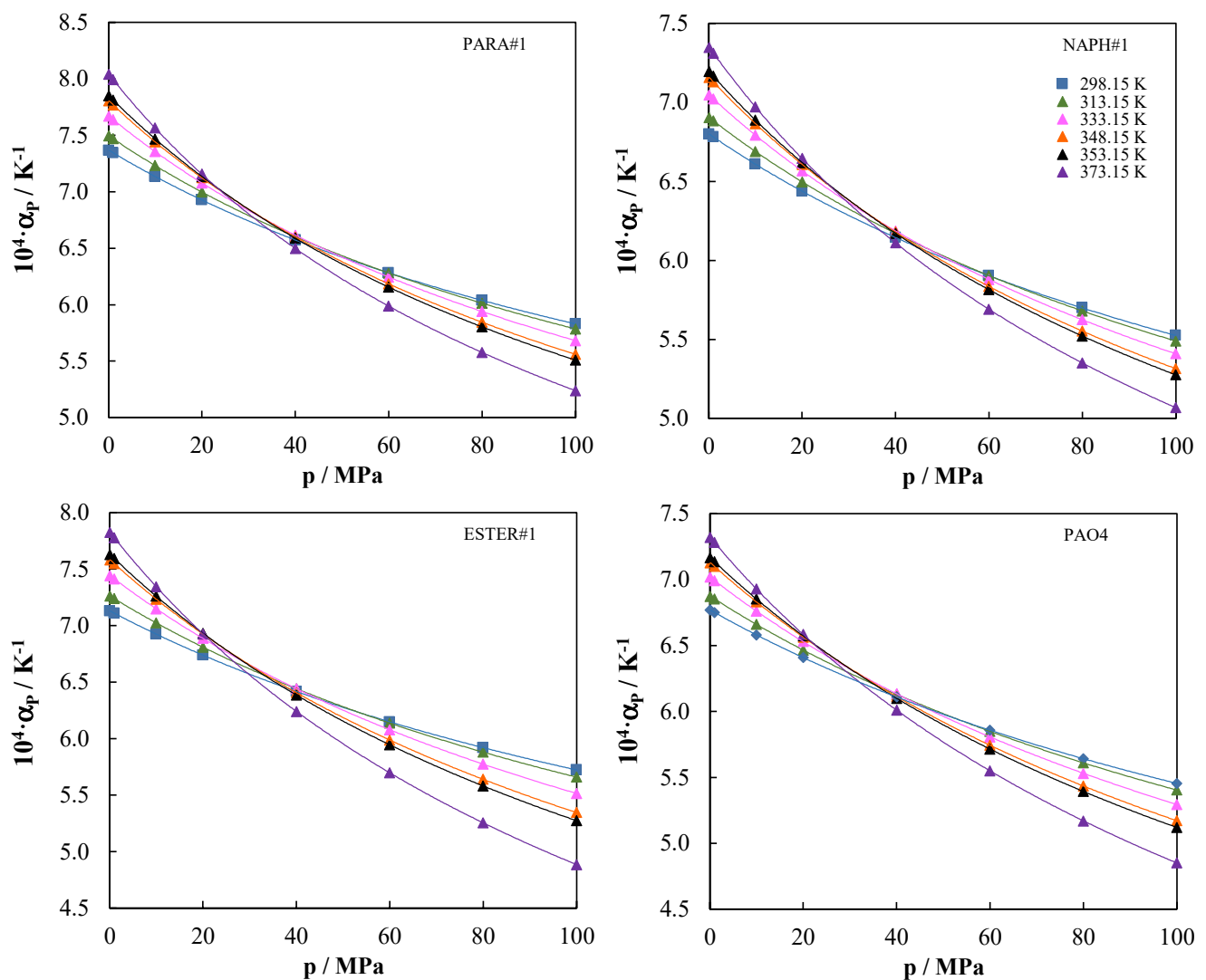


Figure 4. Isobaric thermal expansivities, α_p , with an uncertainty of $0.3 \cdot 10^{-4} \text{ K}^{-1}$ against pressure at different temperatures for the base oils with a low-viscosity grade. The solid lines are for guidance.

However, the data for the low-viscosity base oils revealed a different sequence: ESTER#1 > PARA#1 > NAPH#1 > PAO4; in this case, the contact angle was the highest for the esters base oil (ESTER#1) and the lowest for PAO4. In addition, at 323.15 K, PARA#2 (high-viscosity paraffinic oil) reached the steady-state earlier (approx. 20 s) than the other oils. Figure 8 summarizes the results of the average steady-state contact angles for the AISI 420 stainless steel surface wetted with each of the eight base oils at 298.15 and 323.15 K. The contact angles were between 1.4° and 18.1° at 298.15 K and 0.4° and 14.3° at 323.15 K, for all the base oils. As expected, a reduction in the average steady-state contact angle was observed with the increase in temperature, which was around 69% for PARA#1 (low-viscosity paraffinic oil) and 32% for PAO16. At both temperatures, the lowest contact angles corresponded to PAO4 and the highest to PARA#2 (high-viscosity paraffinic base oil).

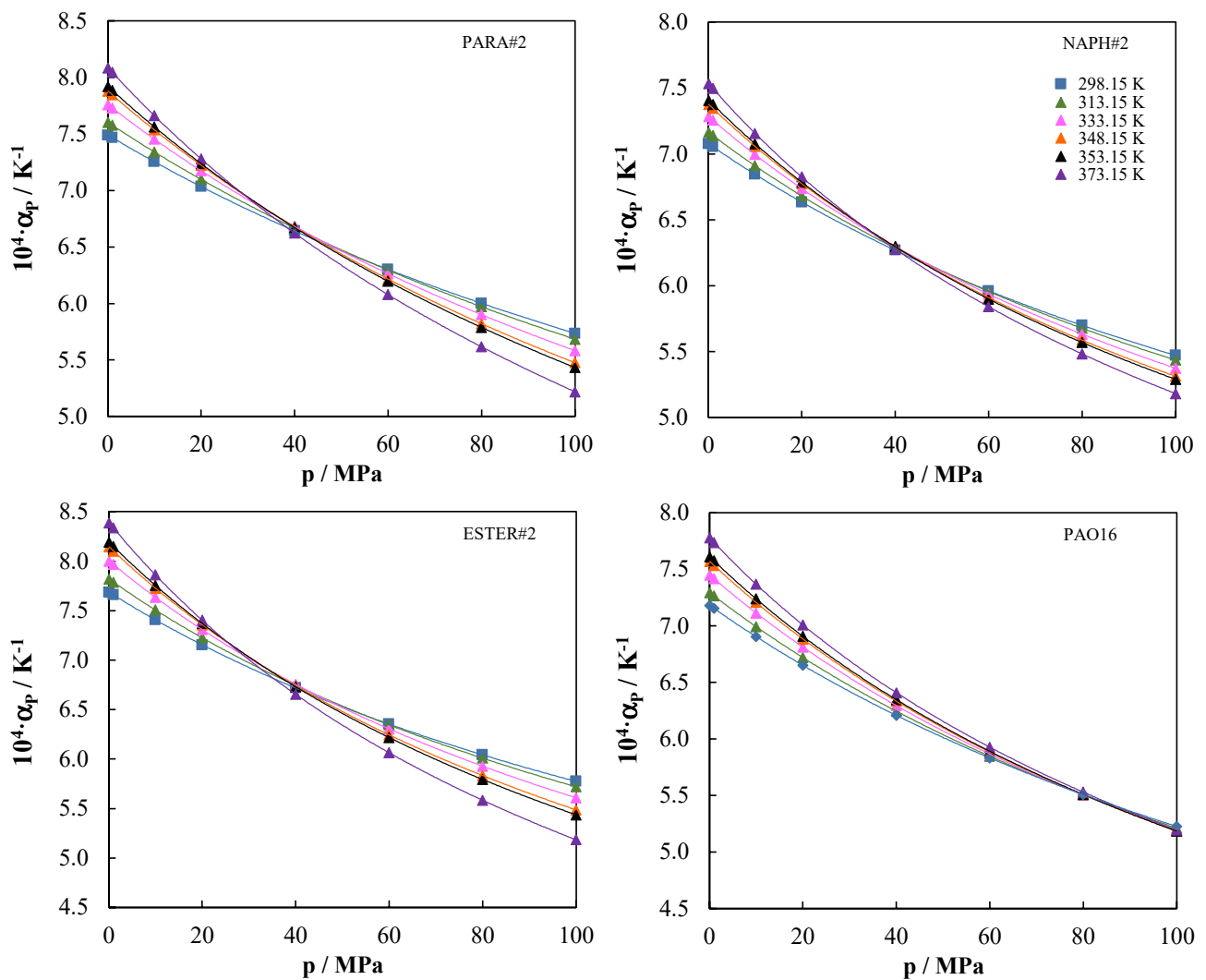


Figure 5. Isobaric thermal expansivities, α_p , with an uncertainty of $0.3 \cdot 10^{-4} \text{ K}^{-1}$ against pressure at different temperatures for the base oils with a high-viscosity grade. The solid lines are for guidance.

Coelho de Sousa Marques et al. [7] measured the contact angle for different base oils on AISI 420 stainless steel surface from 293.15 to 323.15 K. They reported the contact angle for four different polyalphaolefins (PAO6, PAO20, PAO32, and PAO40) and for four ester-based lubricants (TMPTO, TOTM, TTM, and BIOE). These authors [7] measured the contact angle at 5 s after the droplet fall, finding 6.8° and 12.6° for PAO6 and PAO20 at 323.15 K, respectively. In the present work, PAO4 and PAO16 provided contact angles at the same droplet fall time (5 s) and at 323.15 K of 5.4° and 15.0° , respectively. Thus, we observed a good agreement considering the uncertainty of the two measurements.

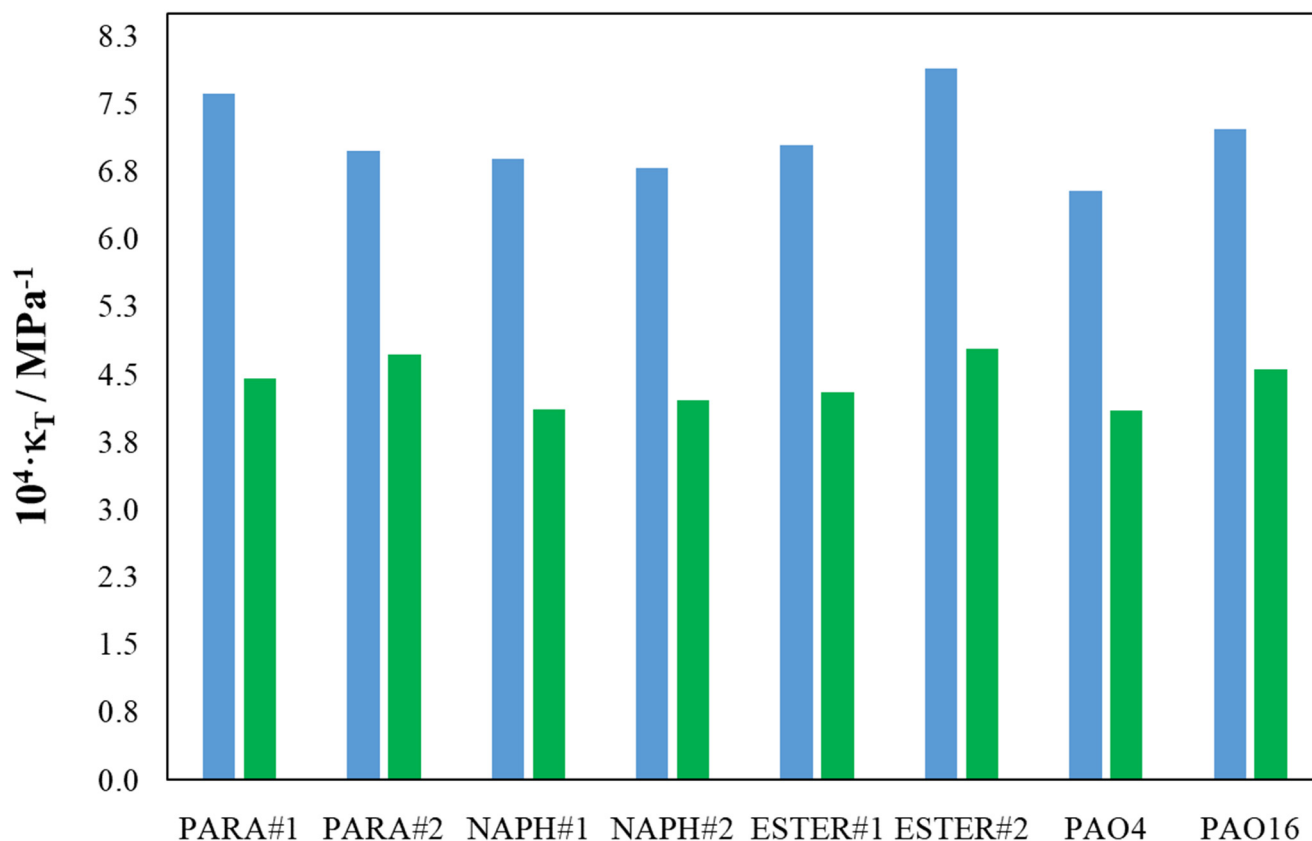


Figure 6. Isothermal compressibility (k_T) values with an uncertainty of $0.06 \cdot 10^{-4} \text{ MPa}^{-1}$ for eight base oils at 333.15 K and (■) 0.1 MPa and (■) 100 MPa.

The kinematic and dynamic viscosities for the eight oils measured with SVM3000 apparatus are reported in Table 1. The dynamic viscosities at 0.1 MPa of all the base oils with low-viscosity grades (PARA#1, NAPH#1, ESTER#1, and PAO4) range along the entire temperature interval, from around 3 mPa s to 187 mPa s. Five of the base oils studied in this work (PARA#1, NAPH#1, ESTER#1, PAO4, and NAPH#2) had kinematic viscosities at 373.15 K and 0.1 MPa, between $3 \text{ mm}^2 \text{ s}^{-1}$ and $10 \text{ mm}^2 \text{ s}^{-1}$, which means that they could be used in the formulation of automatic transmission fluids (ATF) for electric vehicles, with configurations where the ATF and the electric motor are in contact due to the latter being inside the transmission housing [34]. From Figure 9, where the logarithm of the dynamic viscosity is plotted against temperature, we can observe that PARA#1, NAPH#1, and PAO4 had very similar viscosities over the temperature range (343.15–373.15 K). Moreover, the ester oil ESTER#1 presented the higher viscosities within the temperature interval (298.15–373.15 K). On the contrary, at temperatures lower than 298.15 K, the naphthenic oil (NAPH#1) was more viscous than the other three oils; thus, the following trend is obtained: NAPH#1 > ESTER#1 > PARA#1 > PAO4. For the base oils with a high-viscosity grade (PARA#2, NAPH#2, ESTER#2, and PAO16), the dynamic viscosity at 0.1 MPa ranged from 8 mPa s to 2006 mPa s over the entire temperature interval. We observed that, for temperatures lower than 308.15 K, the naphthenic oil (NAPH#2) was more viscous than the other three oils (PARA#2, ESTER#2, and PAO16). Over the entire temperature interval (308.15–318.15 K), the dynamic viscosity of the base oils with a high-viscosity grade were quite similar. However, the trend found for temperatures higher than 318.15 K was PAO16 > ESTER#2 > PARA#2 > NAPH#2.



Figure 7. Images of the sessile drop evolution for all mineral and synthetic oils at 298.15 K.

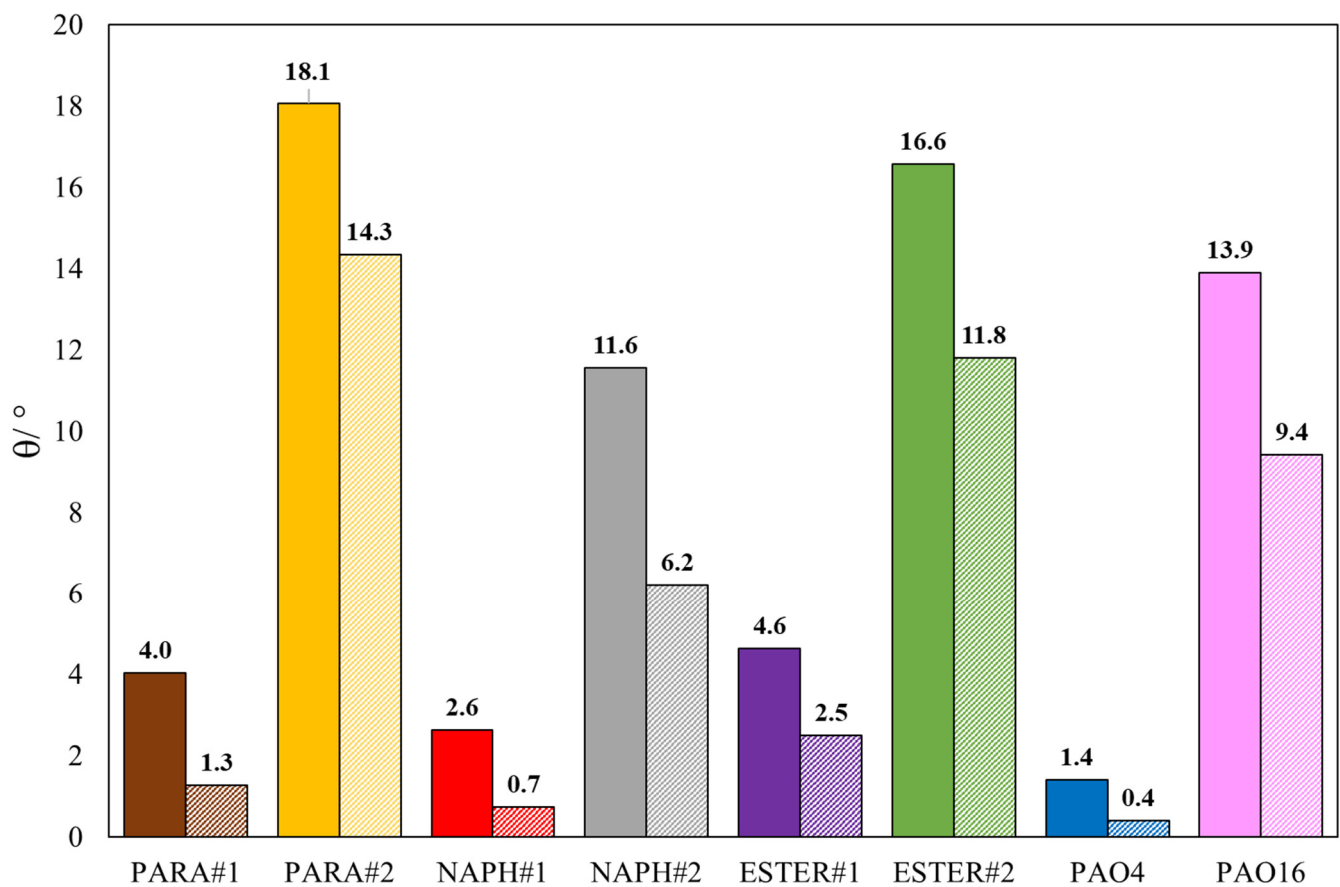


Figure 8. Average steady-state contact angle (θ) of the eight base oils at 298.15 K (filled bars) and 323.15 K (clear bars).

The viscosity index obtained for the eight base oils is reported in Figure 10. The ester and polyalphaolefin oils (synthetic oils) have the highest viscosity index (VI from 122 to 154), that is, they present the lower dependence of the viscosity with the temperature. Both esters have a similar viscosity index (VI = 140), even if both oils have very different viscosity grades. Thus, the viscosity of these synthetic oils is less dependent on temperature changes than that of mineral oils. The very-low values obtained for the VI of the naphthenic base oils were checked measuring the viscosity index three times, obtaining the same results. The VI of the naphthenic base oils indicates that, for these oils, it is necessary to use VI improvers, also known as viscosity modifiers. However, the use of additives as viscosity improvers has some drawbacks, for example, using polymers with a higher molecular weight as additives would improve the thickening properties, but they show less resistance to mechanical shearing. This highlights the great difficulty involved in formulating new lubricants, since the use of one additive can improve one property, but, at the same time, worsen another. In other words, it is necessary to strike a strict balance between the different properties that are to be achieved for the final lubricant.

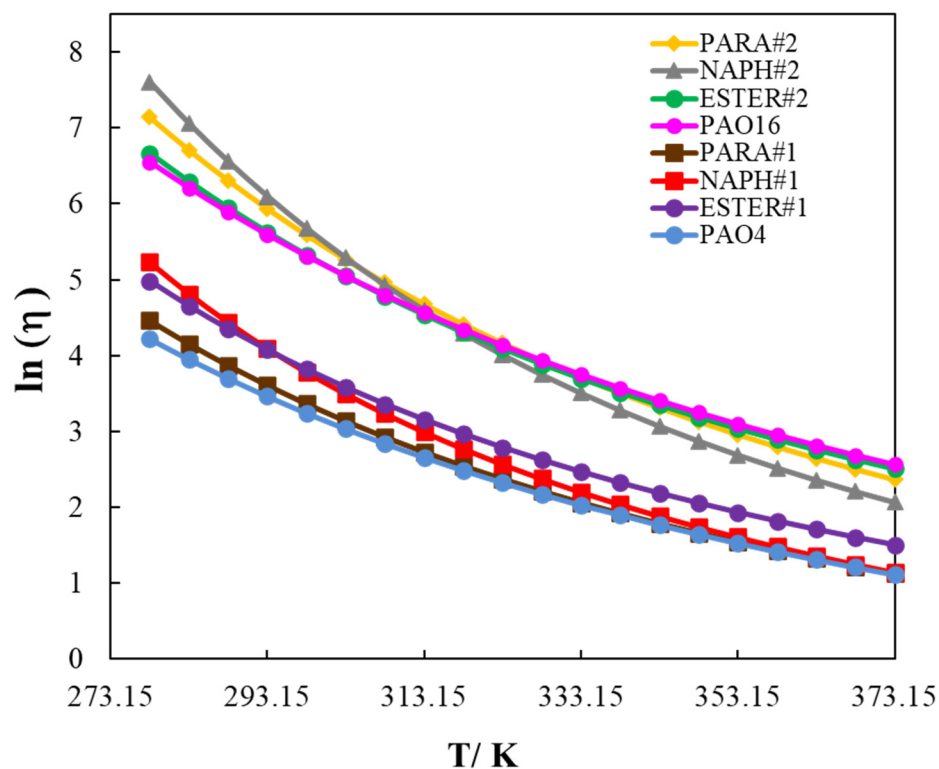


Figure 9. Dynamic viscosity ($\ln \eta$) versus temperature at 0.1 MPa for the eight studied oils.

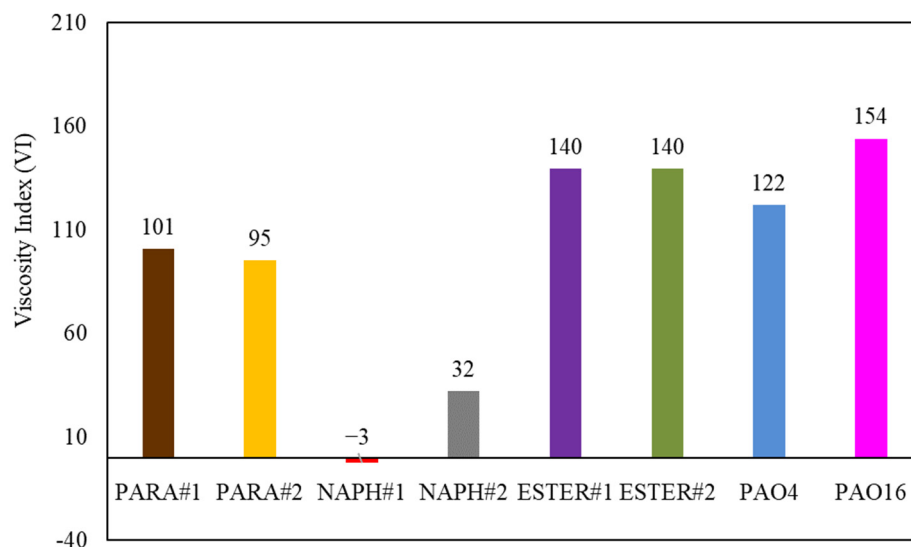


Figure 10. Viscosity index (VI) for the eight studied base oils: four mineral (PARAs and NAPHs) and four synthetic (PAOs and ESTERs) oils.

The dynamic viscosities at high pressures for the eight base oils are reported in Table 6. As Figure 11 shows, at 323.15 K and for pressures lower than 50 MPa, the dependence of the viscosity with pressure was quite similar for the eight oils. For pressures higher than 50 MPa, the bigger increase in the viscosity with pressure occurred for the mineral naphthenic oils: NAPH#2 (viscosity at 150 MPa around 40 times higher than that at 0.1 MPa), followed by NAPH#1 (viscosity at 150 MPa around 30 times higher than that at 0.1 MPa). The studied synthetic polyalphaolefin oils (PAO4 and PAO16) had the lowest dependence of the viscosity with pressure (viscosity at 150 MPa/viscosity at 0.1 MPa ≤ 10). At 353.15 K, for the oils with the highest viscosity grade (PARA#2, NAPH#2, ESTER#2, and

PAO16), the pressure dependence of the viscosity was quite similar, up to 75 MPa. For pressures higher than 75 MPa, once again mineral oils, especially NAPH#2, had the biggest increase in the viscosity with pressure. For the oils with a lower ISO VG grade at 353.15 K, ESTER#1 had the highest viscosity values at a pressure up to 75 MPa and, for pressures higher or equal than 100 MPa, NAPH#1 is the most viscous fluid.

Table 6. Dynamic viscosity, η /mPa s, at different temperatures, T /K, and pressures, P /MPa, measured with the high-pressure falling body viscometer.

T /K	323.15	353.15	323.15	353.15	323.15	353.15	323.15	353.15
P /MPa	PARA#1		PARA#2		NAPH#1		NAPH#2	
10	12.28	5.148	72.35	21.38	14.31	6.005	63.77	16.56
15	13.57	5.614	82.02	23.71	16.57	6.566	72.73	18.21
25	16.42	6.620	103.9	28.85	21.83	7.835	94.19	22.07
50	25.34	9.618	176.5	45.19	40.75	12.09	176.8	36.32
75	37.59	13.47	284.7	68.09	72.21	18.50	327.0	60.77
100	54.41	18.40	446.2	100.2	124.5	28.2	600.3	102.7
125	77.51	24.74	687.1	145.2	211.5	42.7	1098.3	174.8
150	109.3	32.9	1047.1	208.3	356.5	64.7	2006.1	298.7
P /MPa	ESTER#1		ESTER#2		PAO4		PAO16	
10	19.09	7.894	66.80	22.58	11.67	5.132	71.05	25.08
15	20.96	8.534	73.34	24.56	12.69	5.548	78.32	27.20
25	25.09	9.914	87.70	28.83	14.91	6.432	94.14	31.79
50	37.95	14.04	132.5	41.54	21.58	8.971	142.5	45.6
75	55.54	19.36	193.7	57.83	30.25	12.07	206.6	63.4
100	79.58	26.21	277.3	78.70	41.52	15.84	291.6	86.4
125	112.5	35.03	391.6	105.4	56.18	20.44	404.4	116.3
150	157.5	46.41	547.9	139.8	75.24	26.05	554.2	155.0

The experimental dynamic viscosity data as a function of pressure, $\eta(p)$, were fitted using Equation (6), where η_0 is the dynamic viscosity value obtained with the Anton Paar Stabinger viscometer at 0.1 MPa at each temperature (reported in Table 1), and A, B, and C are adjustable parameters. The values of these parameters and the standard deviation of the fit are reported in Table 7. Equation (6) with the values of the parameters of Table 7 reproduces the experimental dynamic viscosity values with a standard deviation lower than 5 mPa s.

Using Equations (6)–(9), the values of α_{film} and α^* at different temperatures for the eight base oils studied in this work were determined. These values are reported in Table 8. As can be observed in Figure 12, the highest α_{film} values were obtained for the naphthenic base oils (NAPH#1 and NAPH#2), followed by the paraffinic oils (PARA#1 and PARA#2). The universal pressure–viscosity coefficient (α_{film}) for ESTER#1, ESTER#2, and PAO16 are very similar, around 15 GPa^{−1} at 323.15 K and around 13 GPa^{−1} at 353.15 K. The lowest α_{film} values were obtained for PAO4. As expected, both coefficients (α_{film} and α^*) decreased with temperature. The values reported in Table 8 agree with the previously published data for other mineral and synthetic oils [25,35].

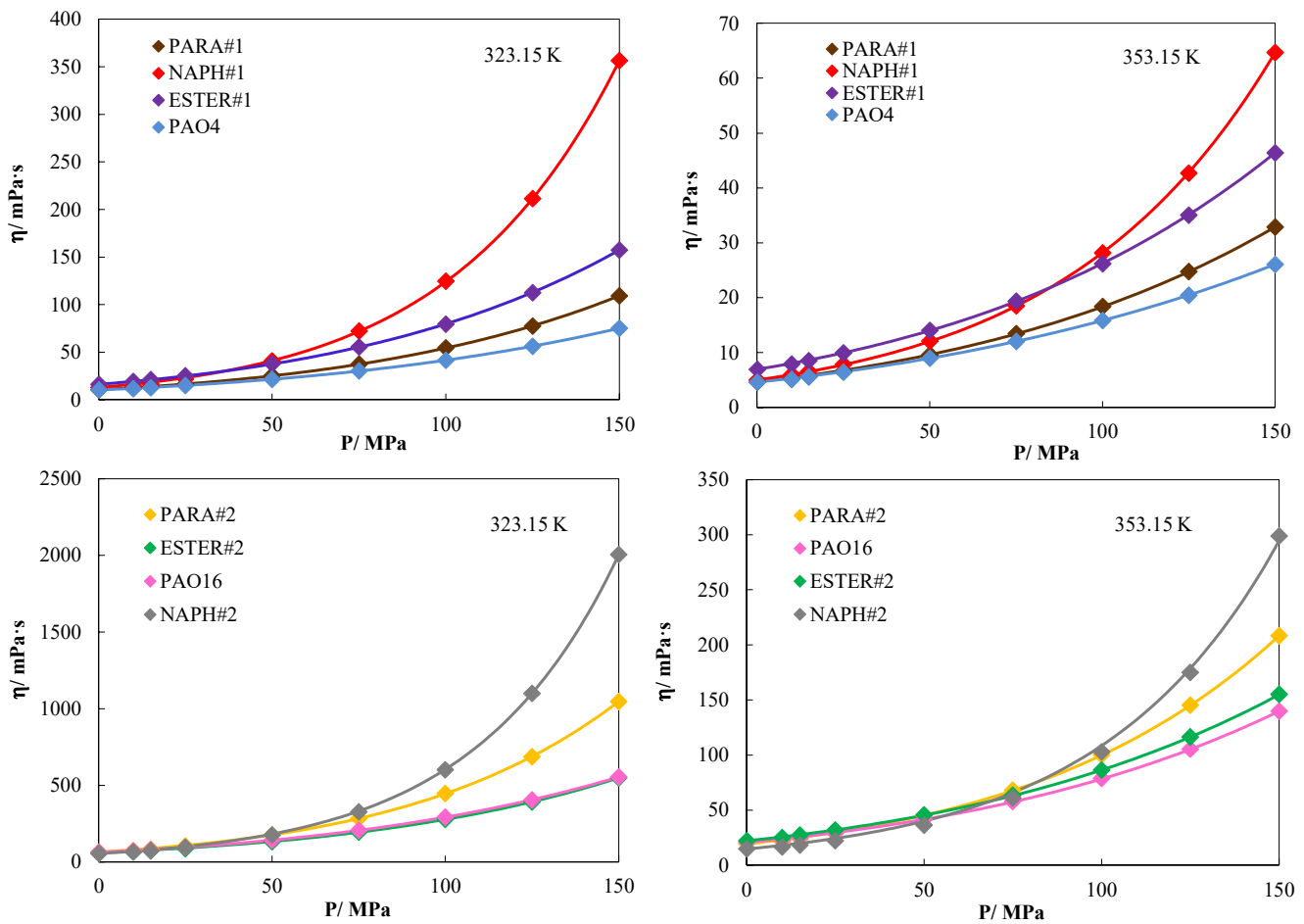


Figure 11. Viscosity as a function of pressure for the eight studied base oils: four mineral (PARAs and NAPHs) and four synthetic (PAOs and ESTERs) oils.

Table 7. Parameters and deviations for the viscosity correlation by using Equation (6).

T/K	323.15	353.15	323.15	353.15	323.15	353.15	323.15	353.15
	PARA#1		PARA#2		NAPH#1		NAPH#2	
A	7.58652	6.11536	11.009	10.431	24.685	30.881	80.8	92.3
B	419.07	398.94	519.04	584.55	1044.62	1733.57	3305.6	4699.7
σ /mPa s	0.3	0.2	3.6	0.9	1.2	0.07	4.7	4.0
	ESTER#1		ESTER#2		PAO4		PAO16	
A	7.219	6.050	9.552	7.041	5.915	4.005	5.893	6.226
B	405.830	405.78	574.04	482.55	373.62	276.70	334.11	408.60
σ /mPa s	0.3	0.07	1.9	0.8	0.15	0.1	1.6	0.3

The pressure–viscosity coefficient of the eight base oils were also determined from the equation proposed by Gold et al. [11]. The kinematic viscosity needed in Equation (10) was obtained from Table 1. The pressure–viscosity coefficients obtained from both the procedure proposed by Bair et al. (α_{film}) and Equation (10) (α_{Gold}) decrease when the temperature rises. It was observed that α_{film} values were higher than the α_{Gold} values for all the base oils studied in this work, except for NAPH#2, for which the α value obtained from the Gold method is around 8% higher than the α_{film} value. For the mineral base oils (PARA#1, PARA#2, NAPH#1, and NAPH#2), average deviations around 10% at 323.15 K and 5% at 353.15 K between α_{film} and α_{Gold} values were found. These deviations are higher for the synthetic base oils (ESTER#1, ESTER#2, PAO4, and PAO16), and thus average deviations around

25% at 323.15 K and 22% at 353.15 K were obtained, respectively. We must emphasize that, in the database used by Gold et al. to determine the s and m parameters, the lubricants used were in the range from ISO VG32 to ISO VG 460, which means they used oils with a kinematic viscosity higher than $30 \text{ mm}^2 \text{ s}^{-1}$ at 313.15 K. As can be observed in Table 1, the kinematic viscosities of PARA#1, NAPH#1, ESTER#1, and PAO4 at 313.15 K were lower than this value.

Table 8. Universal pressure–viscosity coefficient α_{film} and reciprocal asymptotic isoviscous pressure coefficient α^* for the base oils.

Base Oils	T/K	$\alpha_{\text{film}}/\text{GPa}^{-1}$	α^*/GPa^{-1}
PARA#1	323.15	16.3	15.2
	353.15	13.4	12.8
PARA#2	323.15	19.7	19.2
	353.15	16.5	16.1
NAPH#1	323.15	22.8	22.6
	353.15	17.3	17.2
NAPH#2	323.15	24.1	24.1
	353.15	19.4	19.4
ESTER#1	323.15	15.9	15.3
	353.15	13.3	12.4
ESTER#2	323.15	15.3	14.9
	353.15	13.0	12.5
PAO4	323.15	13.8	13.2
	353.15	11.8	11.0
PAO16	323.15	15.4	14.6
	353.15	13.4	12.8

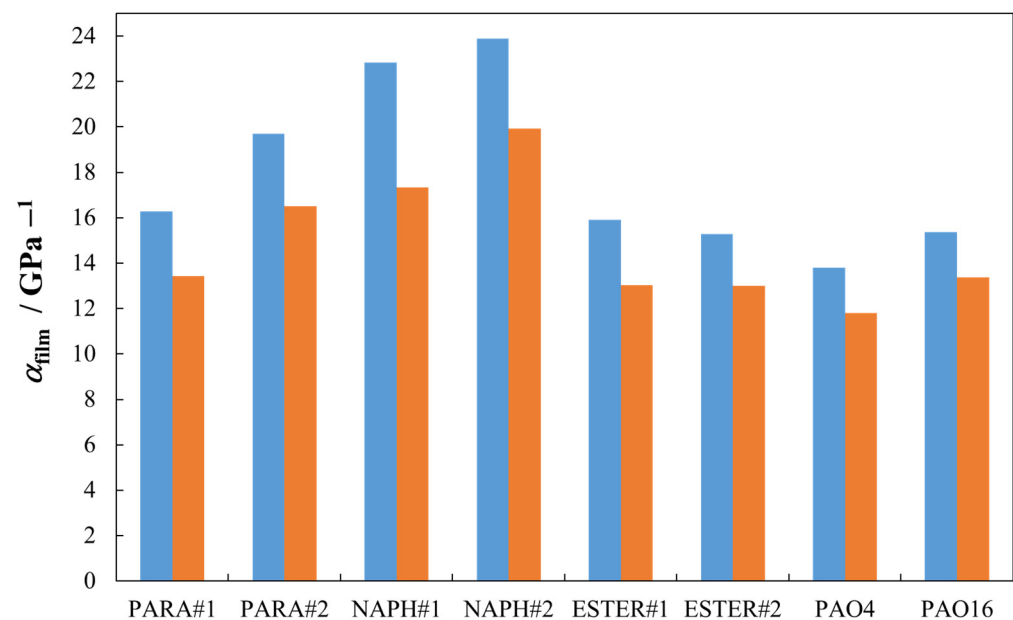


Figure 12. Universal pressure–viscosity coefficient (α_{film}) for the eight studied base oils: four mineral (PARAs and NAPHs) and four synthetic (PAOs and ESTERs) oils. (■) 323.15 K and (■) 353.15 K.

The results obtained for $\eta_0^{0.69} \alpha^{0.56}$ for the eight base oils studied in the present work are shown in Figure 13 at 323.15 K and 353.15 K. At 323.15 K, for the base oils with the highest viscosity (PARA#2, NAPH#2, ESTER#2, and PAO16), we observed that PARA#2 and NAPH#2 had higher values than ESTER#2 and PAO16. This means that, at 323.15 K, the mineral base oils generate a thicker film than the synthetic ones. At 353.15 K, regarding the four high-viscosity oils, PARA#2 and PAO16 had slightly higher $\eta_0^{0.69} \alpha^{0.56}$ values than

NAPH#2 and ESTER#2. For the low-viscosity base oils (PARA#1, NAPH#1, ESTER#1, and PAO4), it can be observed in Figure 13 that NAPH#1 and ESTER#1 presented similar and higher $\eta_0^{0.69} \alpha^{0.56}$ values than PARA#1 and PAO4 for both temperatures 323.15 and 353.15 K. Finally, we must emphasize that the naphthenic base oils presented the highest variation of $\eta_0^{0.69} \alpha^{0.56}$ with temperature, mainly due to their low-viscosity index.

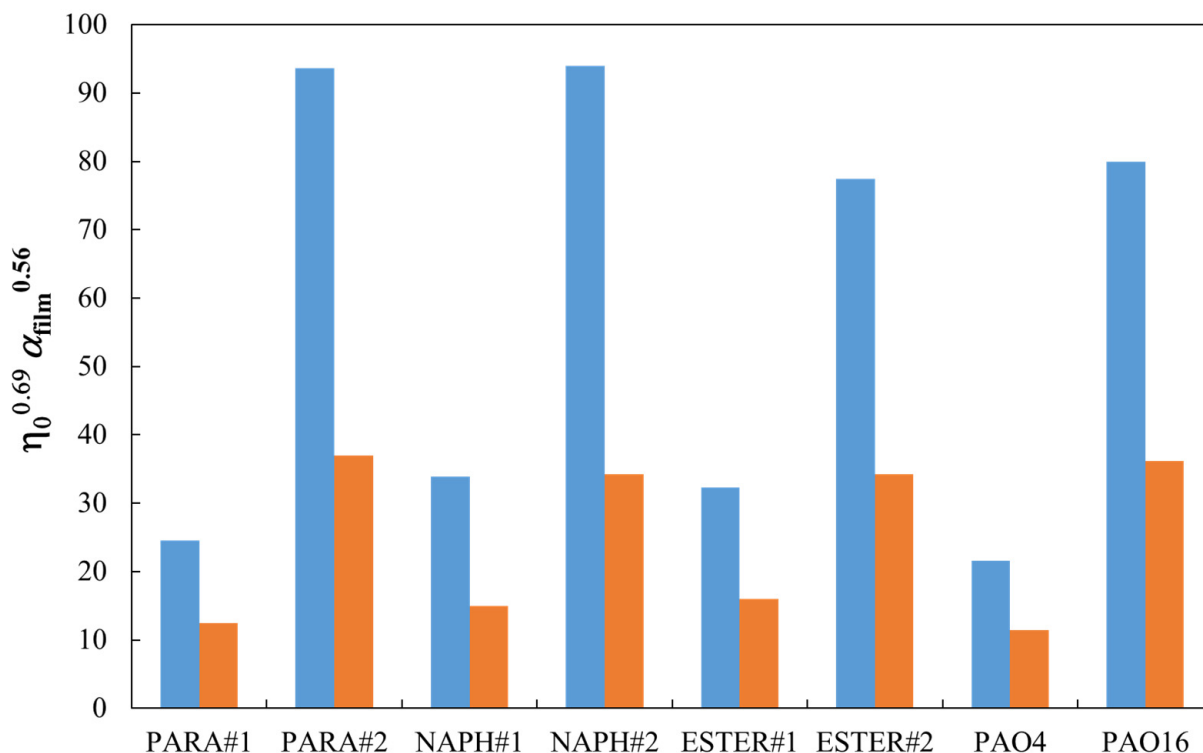


Figure 13. $\eta_0^{0.69} \alpha^{0.56}$ for the eight studied base oils: four mineral (PARAs and NAPHs) and four synthetic (PAOs and ESTERs) oils. (■) 323.15 K and (■) 353.15 K.

4. Conclusions

Several thermophysical properties of eight mineral and synthetic base oils were experimentally determined. The following features were observed:

1. The densities of the synthetic oils were the highest (ESTERs) and the lowest (PAOs) of all the base oils. The following sequence was observed: ESTER > NAPH > PARA > PAO for both the ISO VG22 and ISO VG100 base oils. Densities at 100 MPa were around 5% higher than those at 0.1 MPa for all the base oils for all the isotherms.
2. Decreases with pressure around 20% at 298.15 K and around 35% at 373.15 K were observed for the isobaric thermal expansivity and 35% and 45%, respectively, for the isothermal compressibility, over the range of 0.1–100 MPa. The more compressible base oil was ESTER#2, so a priori, the risk surface fatigue would be lower with this base oil, although this must be verified by performing tribological tests.
3. The lowest contact angle corresponded to PAO4 and the highest to PARA#2. Base oils with an ISO VG100 grade had a higher contact angle than base oils with ISO VG22, which suggests the poorer wetting of the high-viscosity base oils.
4. Mineral naphthenic oils presented the highest increase in the viscosity with pressure and the synthetic polyalphaolefin oils the lowest. The highest α_{film} values were obtained for naphthenic base oils (NAPH#1 and NAPH#2), followed by the paraffinic oils (PARA#1 and PARA#2), with the lowest α_{film} values being obtained for PAO4. Average deviations between 5% and 25% were obtained between the α_{film} and α_{Gold} values for the eight base oils.

- The naphthenic base oils (NAPH#1 and NAPH#2) presented the highest variation of $\eta_0^{0.69}\alpha^{0.56}$ with the temperature, which means that they could diminish the efficiency of the machinery in comparison with other base oils.

Author Contributions: Conceptualization, F.U. and J.F.; methodology, A.V., M.J.G.G., J.M.L.d.R. and F.M.; software, F.M.; validation, M.J.P.C. and A.V.; formal analysis, J.F. and F.U.; investigation, A.V., M.J.G.G., J.M.L.d.R. and M.J.P.C.; resources, F.U. and R.U.; data curation, A.V.; writing—original draft preparation, M.J.P.C.; writing—review and editing, M.J.P.C.; visualization, J.F. and M.J.P.C.; supervision, F.U.; project administration, J.F.; funding acquisition, J.F. and F.U. All authors have read and agreed to the published version of the manuscript.

Funding: This research was funded by MCIN/AEI/10.13039/501100011033 and by the European Regional Development Fund (ERDF, a way of making Europe) through the ENE2017-86425-C2-2-R and the PID2020-112846RB-C22 projects as well as by Xunta de Galicia (ED431C 2020/10). José M. Liñeira del Río acknowledges the grant of the Margarita Salas program, funded by MCIN/AEI/10.13039/501100011033 and “European Union NextGenerationEU/PRTR” María J. G. Guimarey acknowledges a postdoctoral fellowship (ED481B-2019-015) from the Xunta de Galicia (Spain).

Data Availability Statement: Not applicable.

Conflicts of Interest: The authors declare no conflict of interest.

References

- Chowdary, K.; Kotia, A.; Lakshmanan, V.; Elsheikh, A.H.; Ali, M.K.A. A Review of the Tribological and Thermophysical Mechanisms of Bio-Lubricants Based Nanomaterials in Automotive Applications. *J. Mol. Liq.* **2021**, *339*, 116717. [[CrossRef](#)]
- Quinchia, L.; Delgado, M.; Reddyhoff, T.; Gallegos, C.; Spikes, H.A. Tribological Studies of Potential Vegetable Oil-Based Lubricants Containing Environmentally Friendly Viscosity Modifiers. *Tribol. Int.* **2014**, *69*, 110–117. [[CrossRef](#)]
- Boyde, S. Green Lubricants. *Environmental Benefits and Impacts of Lubrication. Green Chem.* **2002**, *4*, 293–307. [[CrossRef](#)]
- Larsen, R.G.; Bondi, A. Functional Selection of Synthetic Lubricants. *Ind. Eng. Chem.* **1950**, *42*, 2421–2427. [[CrossRef](#)]
- Leslie, R. *Rudnick Synthetics, Mineral Oils, and Bio-Based Lubricants Chemistry and Technology*; CRC Press: Boca Raton, FL, USA, 2020; ISBN 978-1-138-06821-6.
- Nagendramma, P.; Kaul, S. Development of Ecofriendly/Biodegradable Lubricants: An Overview. *Renew. Sustain. Energy Rev.* **2012**, *16*, 764–774. [[CrossRef](#)]
- Coelho de Sousa Marques, M.A.; Guimarey, M.J.G.; Domínguez-Arca, V.; Amigo, A.; Fernández, J. Heat Capacity, Density, Surface Tension, and Contact Angle for Polyalphaolefins and Ester Lubricants. *Thermochim. Acta* **2021**, *703*, 178994. [[CrossRef](#)]
- Totten, G.; Westbrook, S.; Shah, R. *Fuels and Lubricants Handbook: Technology, Properties, Performance, and Testing*; ASTM International: West Conshohocken, PA, USA, 2003.
- Besanjideh, M.; Nassab, S.A.G. Effect of Lubricant Compressibility on Hydrodynamic Behavior of Finite Length Journal Bearings Running under Heavy Load Conditions. *J. Mech.* **2016**, *32*, 101–111. [[CrossRef](#)]
- Bronshteyn, L.A.; Kreiner, J.H. Energy Efficiency of Industrial Oils. *Tribol. Trans.* **1999**, *42*, 771–776. [[CrossRef](#)]
- Gold, P.W.; Schmidt, A.; Dicke, H.; Loos, J.; Assmann, C. Viscosity–Pressure–Temperature Behaviour of Mineral and Synthetic Oils. *J. Synth. Lubr.* **2001**, *18*, 51–79. [[CrossRef](#)]
- Fernández Rico, E.; Minondo, I.; García Cuervo, D. Rolling Contact Fatigue Life of AISI 52100 Steel Balls with Mineral and Synthetic Polyester Lubricants with PTFE Nanoparticle Powder as an Additive. *Wear* **2009**, *266*, 671–677. [[CrossRef](#)]
- Grandelli, H.E.; Dickmann, J.S.; Devlin, M.T.; Hassler, J.C.; Kiran, E. Volumetric Properties and Internal Pressure of Poly(α -Olefin) Base Oils. *Ind. Eng. Chem. Res.* **2013**, *52*, 17725–17734. [[CrossRef](#)]
- Dickmann, J.S.; Devlin, M.T.; Hassler, J.C.; Kiran, E. High Pressure Volumetric Properties and Viscosity of Base Oils Used in Automotive Lubricants and Their Modeling. *Ind. Eng. Chem. Res.* **2018**, *57*, 17266–17275. [[CrossRef](#)]
- Wang, Y.; Fernandez, J.E.; Cuervo, D.G. Rolling-Contact Fatigue Lives of Steel AISI 52100 Balls with Eight Mineral and Synthetic Lubricants. *Wear* **1996**, *196*, 110–119. [[CrossRef](#)]
- Teh, J.L.; Walvekar, R.; Nagarajan, T.; Said, Z.; Khalid, M.; Mubarak, N.M. A Review on the Properties and Tribological Performance of Recent Non-Aqueous Miscible Lubricants. *J. Mol. Liq.* **2022**, *366*, 120274. [[CrossRef](#)]
- Segovia, J.J.; Fandiño, O.; López, E.R.; Lugo, L.; Carmen Martín, M.; Fernández, J. Automated Densimetric System: Measurements and Uncertainties for Compressed Fluids. *J. Chem. Thermodyn.* **2009**, *41*, 632–638. [[CrossRef](#)]
- Dakkach, M.; Gaciño, F.M.; Guimarey, M.J.G.; Mylona, S.K.; Paredes, X.; Comuñas, M.J.P.; Fernández, J.; Assael, M.J. Viscosity-Pressure Dependence for Nanostructured Ionic Liquids. Experimental Values for Butyltrimethylammonium and 1-Butyl-3-Methylpyridinium Bis(Trifluoromethylsulfonyl)Imide. *J. Chem. Thermodyn.* **2018**, *121*, 27–38. [[CrossRef](#)]

19. Guimarey, M.J.G.; Abdelkader, A.M.; Comuñas, M.J.P.; Alvarez-Lorenzo, C.; Thomas, B.; Fernández, J.; Hadfield, M. Comparison between Thermophysical and Tribological Properties of Two Engine Lubricant Additives: Electrochemically Exfoliated Graphene and Molybdenum Disulfide Nanoplatelets. *Nanotechnology* **2021**, *32*, 025701. [[CrossRef](#)]
20. Zhang, L.; He, Y.; Zhu, L.; Yang, C.; Niu, Q.; An, C. In Situ Alkylated Graphene as Oil Dispersible Additive for Friction and Wear Reduction. *Ind. Eng. Chem. Res.* **2017**, *56*, 9029–9034. [[CrossRef](#)]
21. van Leeuwen, H. The Determination of the Pressure–Viscosity Coefficient of a Lubricant through an Accurate Film Thickness Formula and Accurate Film Thickness Measurements. *Proc. Inst. Mech. Eng. Part J J. Eng. Tribol.* **2009**, *223*, 1143–1163. [[CrossRef](#)]
22. Spikes, H.A.; Hammond, C.J. The Elastohydrodynamic Film Thicknesses of Binary Ester–Ether Mixtures. *A S L E Trans.* **1981**, *24*, 542–548. [[CrossRef](#)]
23. Bair, S.; Liu, Y.; Wang, Q.J. The Pressure-Viscosity Coefficient for Newtonian EHL Film Thickness With General Piezoviscous Response. *J. Tribol.* **2006**, *128*, 624–631. [[CrossRef](#)]
24. Kumar, P.; Bair, S.; Krupka, I.; Hartl, M. Newtonian Quantitative Elastohydrodynamic Film Thickness with Linear Piezoviscosity. *Tribol. Int.* **2010**, *43*, 2159–2165. [[CrossRef](#)]
25. Paredes, X.; Fandiño, O.; Pensado, A.S.; Comuñas, M.J.P.; Fernández, J. Pressure–Viscosity Coefficients for Polyalkylene Glycol Oils and Other Ester or Ionic Lubricants. *Tribol. Lett.* **2012**, *45*, 89–100. [[CrossRef](#)]
26. Höglund, E. Influence of Lubricant Properties on Elastohydrodynamic Lubrication. *Wear* **1999**, *232*, 176–184. [[CrossRef](#)]
27. Larsson, R.; Kassfeldt, E.; Byheden, Å.; Norrby, T. Base Fluid Parameters for Elastohydrodynamic Lubrication and Friction Calculations and Their Influence on Lubrication Capability. *J. Synth. Lubr.* **2001**, *18*, 183–198. [[CrossRef](#)]
28. Cardoso, N.F.R.; Martins, R.C.; Seabra, J.H.O.; Igartua, A.; Rodríguez, J.C.; Luther, R. Micropitting Performance of Nitrided Steel Gears Lubricated with Mineral and Ester Oils. *Tribol. Int.* **2009**, *42*, 77–87. [[CrossRef](#)]
29. Randzio, S.L.; Grolier, J.P.E.; Quint, J.R.; Eatough, D.J.; Lewis, E.A.; Hansen, L.D. N-Hexane As a Model for Compressed Simple Liquids. *Int. J. Thermophys.* **1994**, *15*, 415–441. [[CrossRef](#)]
30. Randzio, S.L. From Calorimetry to Equations of State. *Chem. Soc. Rev.* **1995**, *24*, 359–366. [[CrossRef](#)]
31. Deiters, U.K.; Randzio, S.L. The Equation of State for Molecules with Shifted Lennard-Jones Pair Potentials. *Fluid Phase Equilib.* **1995**, *103*, 199–212. [[CrossRef](#)]
32. Taravillo, M.; Baonza, V.G.; Cáceres, M.; Núñez, J. Thermodynamic Regularities in Compressed Liquids: I. The Thermal Expansion Coefficient. *J. Phys. Condens. Matter* **2003**, *15*, 2979. [[CrossRef](#)]
33. Troncoso, J.; Navia, P.; Romani, L.; Bessieres, D.; Lafitte, T. On the Isobaric Thermal Expansivity of Liquids. *J. Chem. Phys.* **2011**, *134*, 94502. [[CrossRef](#)] [[PubMed](#)]
34. Tuero, A.G.; Sanjurjo, C.; Rivera, N.; Viesca, J.L.; González, R.; Battez, A.H. Electrical Conductivity and Tribological Behavior of an Automatic Transmission Fluid Additised with a Phosphonium-Based Ionic Liquid. *J. Mol. Liq.* **2022**, *367*, 120581. [[CrossRef](#)]
35. Guimarey, M.J.G.; Gonçalves, D.E.P.; Liñeira del Río, J.M.; Comuñas, M.J.P.; Fernández, J.; Seabra, J.H.O. Lubricant Properties of Trimethylolpropane Trioleate Biodegradable Oil: High Pressure Density and Viscosity, Film Thickness, Stribeck Curves and Influence of Nanoadditives. *J. Mol. Liq.* **2021**, *335*, 116410. [[CrossRef](#)]

Disclaimer/Publisher’s Note: The statements, opinions and data contained in all publications are solely those of the individual author(s) and contributor(s) and not of MDPI and/or the editor(s). MDPI and/or the editor(s) disclaim responsibility for any injury to people or property resulting from any ideas, methods, instructions or products referred to in the content.